A heat and mass transport model of clay pot evaporative coolers for vegetable storage

Danyal Rehman [a,d,1], Ethan McGarrigle [b,d,1], Leon Glicksman [c,d], Eric Verploegen [d,*]

[a] Department of Mechanical Engineering, Massachusetts Institute of Technology, Cambridge, MA 02139, USA
[b] Department of Chemical Engineering, Massachusetts Institute of Technology, Cambridge, MA 02139, USA
[c] Department of Architecture, Massachusetts Institute of Technology, Cambridge, MA 02139, USA
[d] D-Lab, Massachusetts Institute of Technology, Cambridge, MA 02139, USA

ARTICLE INFO

ABSTRACT

Clay pot coolers are low-cost technologies that can prolong vegetable shelf-life by providing a cool and humid storage environment through evaporative cooling. A predictive performance model of these systems is not available for investigating the impact of design modifications on device performance. This study proposes transport models for pot-in-pot and pot-in-dish coolers that have been validated with experimental data from 17 field trials from Mali and Rwanda with maximum errors of less than 6% observed. Results show that the pot-in-pot and pot-in-dish devices consume 1.96 and 2.85 L/day of water, respectively. A parametric study was conducted to evaluate how the refrigeration efficiency and daily water consumption are affected by the size of the device, local wind speed, and the mass of vegetables stored in the cooler. Increasing local wind speeds provides a net positive impact on refrigeration efficiency despite the increased convective heating. In addition, the quantity of vegetable mass showed a negligible impact on daily water consumption. Insights from the model suggest that water consumption is more efficient for larger devices.

1. Introduction

Evaporative cooling systems are a promising means for providing refrigeration without the use of fuels or refrigerants. Their benefits generally include reduced energy requirements relative to standard refrigeration systems, lower capital costs, and potential water savings [1]. With increasing global surface temperatures, the demand for passive refrigeration will rise over the upcoming decades [2,3]. In resource-constrained settings, access to a stable electricity grid is often unavailable, requiring an alternative, renewable energy source for sustainable system operation [4]. Evaporative cooling systems perform best in hot and arid regions that include the African Sahel region, home to over 150 million people, of whom the vast majority live in rural areas with limited or unaffordable access to electricity. Evaporative cooling technologies are particularly useful for postharvest vegetable storage of products that are optimally stored in a cool and high humidity environment – including tomatoes, leafy greens, and eggplants [3,5,6].

Food loss is a particular challenge for horticulture producers in developing countries, where an estimated 30–50% of vegetables are lost from farm to fork [6,7]. A lack of access to cooling technologies can lead to the reduced shelf life of crops. This decline in yield can arise due to long transportation times, sub-optimal ambient storage conditions, and insect infestations. As a result, vegetable spoilage contributes to reduced incomes and market access for smallholder farmers [8].

A low cost method of evaporative cooling comes from clay pot coolers. Two common variants are the clay pot in a clay pot (pot-in-pot), commonly referred to as "Zeer pots," and the clay pot in a plastic dish (pot-in-dish) devices shown in Fig. 1 [9]. Both devices use a clay pot for vegetable storage, a wet cloth as an evaporation surface and lid, and a sand layer that serves as the medium for water storage. The device variants differ in their exterior storage vessels. In the pot-in-pot variant, the exterior pot serves as an evaporation surface. For the plastic dish in the pot-in-dish variant, due to its low water permeability, no evaporation occurs from its surface. Evaporation however, does occur from the exposed top surface of the sand in the pot-in-dish configuration. Other established methods of evaporative cooling in the developing world include brick cooling chambers and charcoal cooling chambers [8]; both of

* Corresponding author.
 E-mail addresses: drehman@mit.edu (D. Rehman), ethanmcg@mit.edu (E. McGarrigle), glicks@mit.edu (L. Glicksman), ericv@mit.edu (E. Verploegen).
 [1] These authors contributed equally to this work.

Nomenclature

Physical Constants	Stefan-Boltzmann constant 5.67×10^{-8} W m^{-2} K^{-4}
γ	Surface tension of water at 25 °C 0.0728 N m^{-1}
g	Gravitational acceleration 9.81 m s^{-2}
ΔH_v	Enthalpy of vapourization of water at 25 °C 2.26 $\times$ 10^6 J kg^{-1}
r_i	Radius of device sub-section i [m]
H_i	Height of device sub-section i [m]
k_i	Thermal conductivity of material in sub-section i [W m^{-1} K^{-1}]
ρ_i	Density of material in sub-section i [kg m^{-3}]
$c_{v,i}$	Heat capacity at constant volume of sub-section i [J kg^{-1} K^{-1}]
$\mathbb{V}_i$	Volume of sub-section i [m^3]
ε_i	Emissivity of surface i
T_i	Temperature of sub-section i [K]
$\dot{Q}_{in}$	Heat current flowing into a sub-section [W]
$\dot{Q}_{out}$	Heat current flowing out of a sub-section [W]
N_{H_2O}	Moles of water in the device [mol]
N_s	Total number of evaporation surfaces
$N''_{evap,i}$	Evaporative molar flux of water from sub-section i [mol m^{-2} s^{-1}]
$A_{evap,i}$	Surface area participating in evaporation from sub-section i [m^2]
$\dot{Q}_{evap}$	Heat flux removed due to evaporation [W m^{-2}]
h_m	Convective mass transfer coefficient [m s^{-1}]
M_{r,H_2O}	Molar mass of water [kg mol^{-1}]
R	Universal gas constant [J mol^{-1} K^{-1}]
$p_{sat}(T)$	Saturation pressure of water evaluated at temperature T [Pa]
T_s	Temperature at the surface of evaporation [K]
T_∞	Temperature of the ambient air [K]
RH_∞	Relative humidity of the ambient air
h	Convective heat transfer coefficient [W m^{-2} K^{-1}]
Le	Lewis number
$\mathfrak{F}_{ij}$	View factor between surface i and j
A_g	Area of the ground inside the house [m^2]
A_o	Area of the outer surfaces of the dwelling walls and roof [m^2]
A_s	Area of the device external surfaces [m^2]
ε_g	Emissivity of the ground inside the house
ε_o	Emissivity of the outer surfaces of the dwelling walls and roof
ε_s	Emissivity of the device external surfaces
T_g	Temperature of the ground [K]
T_o	Temperature of the outer surfaces of the house walls/roof [K]
CC	Cloud cover factor
T_{sky}	Sky temperature due to long-wave radiation [K]
a	Scaled dew-point factor
h_c	Height of capillary rise [m]

A_c	Cylindrical annulus cross-sectional area [m^2]
κ	Darcy permeability [m^2]
R_{eff}	Effective pore radius of the clay [m]
θ_s	Contact angle of wetted solid
ε	Clay porosity
μ	Dynamic viscosity of water [Pa s]
$N''_{evap,2}$	Evaporative molar flux from the inner pot [mol m^{-2} s^{-1}]
T_{inside}	Temperature of the inner chamber air [K]
$T_{wet\,bulb}$	Wet bulb temperature [K]
η_c	Refrigeration efficiency
$\tilde{\eta}_c$	Time-averaged refrigeration efficiency
t_{start}	Simulation start time [s]
t_{end}	Simulation end time [s]
$\tilde{m}$	Time-averaged evaporation rate [L day^{-1}]
Bi$_i$	Biot number of a sub-section i
Nu	Nusselt number
Re	Reynolds number
Pr	Prandtl number

which are classified as larger scale evaporative cooling chambers (ECCs) that are not the primary modelling focus of this study.

Both of these devices use evaporative cooling as a mechanism to reduce the temperatures within the interior clay pot. The water added to the sand diffuses bi-directionally through the clay pots to simultaneously increase the relative humidity inside the inner clay pot and evaporate from the surface of the exterior clay pot. Both effects contribute to extending vegetable shelf life [6].

Previous work to model clay pot coolers provides insights into the devices' operational characteristics. These include time taken for the inner chamber to cool, contributions of each heat transfer mode, and overall water consumption. Although there is some literature present on modelling these clay pot coolers, a detailed and validated transport model is not present to the best of the authors' knowledge.

Jaconelli and Palm's model was one of the first preliminary transient heat and mass transfer models to capture the evaporative cooling behaviour [10]. The model, however, is not validated with experimental data from the field. In addition, it assumes constant environmental conditions that are not representative of typical ambient environments. The approach used by the model also fails to account for the radiative heat exchange between the surroundings and the device by neglecting the view factors for indoor devices.

Nwankwojike *et al.* provided a mechanistic model to predict the water-replenishment rate of clay pot cooling technologies [11]. The model is not validated by experiments or field data and the approach introduces a permeability correction factor to estimate the evaporation rate. While this approach is frequently used, it is not accurate in capturing the real-world physics and may provide inaccurate quantifications of the water evaporation rates. Scaling this permeability correction factor for different types of clay or system geometries is also challenging due to the difficulty involved in its quantification.

Date developed a steady state simulation using Reynolds flow model to capture the effects of evaporative cooling [12]. This modelling approach is detailed enough to capture overall system behaviour, however, the studies conducted do not investigate the impact of temporal variations in ambient conditions and oversimplify the systems boundary conditions. This study also does not contain any experimental validation, which makes it difficult to verify the accuracy of the results and parametric studies presented.

Yanhua *et al.* approached the problem through a computational fluid dynamics (CFD) simulation of a large scale evaporative

Fig. 1. Labelled clay pot in plastic dish (pot-in-dish, right) and clay pot in clay pot (pot-in-pot, left) device used from rural households in Mali (cloth not shown).

cooling chamber [13]. While this model shows promise in capturing the spatio-temporal temperature distribution in the chamber, the study lacks model validation through experiments. The modelling itself is also in need of simulation validation through mesh-independence studies or other forms of error quantification.

In this paper an experimentally validated transport model is proposed to provide insights into the key design considerations of these clay pot coolers. Experimental validation is conducted based on data obtained by MIT D-Lab through research projects that evaluated the performance of clay pot coolers in the rural regions of Mali and Rwanda [6,14]. The data from the study in Mali was collected between March (the dry season) and July of 2017 in households in the Mopti region as well as research facilities in the Bamako region of Mali. The data obtained in Rwanda was collected from three locations (Mulindi, Rubona, and Busogo) between February and April 2019. Electronic sensors (provided by Sensen) recorded the ambient temperature, ambient relative humidity, interior chamber temperature, interior chamber relative humidity, and sand moisture, all at 5 minute intervals. The ambient temperature and relative humidity data obtained from these trials were used as inputs to the model to predict system performance. Given the availability of field data for the smaller clay pot coolers, modelling efforts were focused on the smaller-scale systems. Parametric studies have also been included and serve as a platform to inform the design of larger scale devices.

2. Model

2.1. Clay pot cooler geometry

A system model for two clay pot cooler geometries is proposed: the "clay pot in a clay pot (pot-in-pot)" and the "clay pot in a plastic dish (pot-in-dish)". Both clay pot coolers were modelled as a series of nested concentric cylindrical solids in contact. A cylindrical reference frame was selected given the pot geometries where the convention for the z-direction acts upwards. A simplified geometry is shown in Fig. 2 and Fig. 3 for the pot-in-pot and pot-in-dish systems, respectively. Although the devices in reality (presented in Fig. 1) are not perfectly cylindrical, the tapers observed in the clay pot coolers in Mali and Rwanda are usually very steep. For modelling purposes the geometries were assumed to be perfect cylinders with vertical sides. Each region, labelled with roman numerals, represents a different sub-section and material.

Evaporative heat transfer boundary conditions were assigned to occur off the exterior clay pots and the lid for the pot-in-pots. For the pot-in-dish variant the evaporation occurs off the surface of
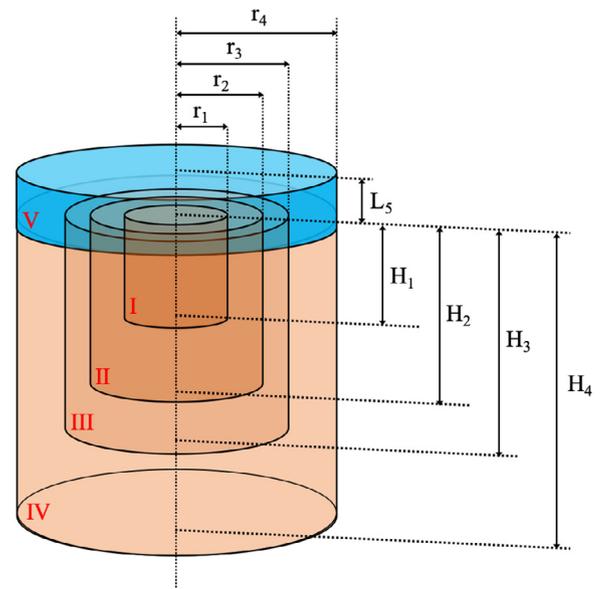

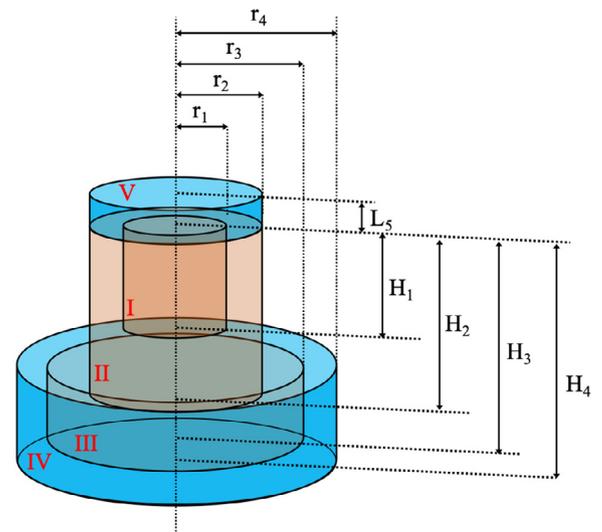**Fig. 2.** Geometric setup of a pot-in-pot system (not to scale).

Fig. 3. Geometric setup of a pot-in-dish system (not to scale).

Table 1

Values of geometric and material thermal properties (pot-in-pot base case properties) [15–17].

Section	$k\left[\frac{W}{mK}\right]$	$\rho\left[\frac{kg}{m^3}\right]$	$c_p\left[\frac{J}{kgK}\right]$	ε [-]	r [m]	H [m]
I (humid air)	0.0257	1.2	1007	-	0.105	0.160
II (interior pot)	1.3	2250	900	-	0.120	0.190
III (sand layer)	3.27	2057	1533	-	0.160	0.270
IV (exterior pot)	2.00	2250	2423	0.775	0.175	0.300
V (wet surface cloth)	0.44	1460	1360	0.770	0.175	0.0025

Table 2

Values of geometric and material thermal properties (pot-in-dish base case properties). Vertical sand thicknesses for the pot-in-dish devices were set at $t_s = 0.035$ cm. The radial thicknesses for both pot-in-pot and pot-in-dish systems can be determined using the difference between H_3 and H_2 [18].

Section	$k\left[\frac{W}{mK}\right]$	$\rho\left[\frac{kg}{m^3}\right]$	$c_p\left[\frac{J}{kgK}\right]$	ε [-]	r [m]	H [m]
I (humid air)	0.0257	1.2	1007	-	0.167	0.360
II (interior pot)	1.3	2250	900	0.775	0.187	0.380
III (sand layer)	3.27	2057	1533	0.760	0.237	0.415
IV (LDPE dish)	0.16	946	2800	0.950	0.240	0.418
V (wet surface cloth)	0.44	1460	1360	0.770	0.240	0.0025

the sand, the inner clay pot, and the lid. Evaporation was not considered off of the dish's surface given the dish's low water permeability. Additional heat flows into and out of the system are detailed in further sections.

The geometric and thermal properties of each sub-section are summarized in Table 1 and 2 below for both design configurations. These values represent a base case which serves as a reference point for the parametric studies conducted in the results and discussion section. The geometric values for both systems were initially provided to a clay potter to build correctly dimensioned devices. These same geometric values were used as an input to the model. These values were kept constant throughout the course of the study. The thermal properties of the humid air were varied over time depending on the temperature of the inner chamber at a given time step using data from psychrometric charts. All other thermal properties were considered time-independent. Performance sensitivity to some of these parameters was considered during the sensitivity analysis and is detailed in later sections.

2.2. Governing equations

2.2.1. Energy balance

The first law of thermodynamics was applied to each sub-section of the clay pot coolers. The energy balance considers a control volume encompassing each sub-section. This assumes a constant and uniform temperature distribution within each sub-section at any given instant in time. This assumption was justified by calculating the Biot numbers for each sub-section and ensuring that their values were below 0.1 (see supplementary information). The energy balance can be found in Eq. (1) below:

$$\frac{d}{dt}\left(\rho_i \mathbb{V}_i c_{v,i} T_i\right) = \sum_i \dot{Q}_{in} - \sum_i \dot{Q}_{out} \tag{1}$$

where ρ_i is the density of sub-section i, $\mathbb{V}_i$ is its volume, $c_{v,i}$ is its specific heat capacity, and T_i is its temperature. $\dot{Q}_{in}$ and $\dot{Q}_{out}$ represent the heat inputs and outputs of the sub-sections, respectively. The heat flows into and out of the system already account for the enthalpy of the evaporating water from the devices. This is detailed further in Section 2.2.3. At the start of each simulation, the temperatures of all sub-sections were initialized in thermal equilibrium with the observed inner chamber temperature. For devices filled with vegetables, the inner chamber was discretized into two sub-sections (humid air and vegetables), using the same lumped approach provided in Eq. (1). The air and vegetable thermal masses

were determined from vegetable mass specifications and vegetable thermal properties [19].

The heat inputs and outputs were calculated by considering interfacial heat transfer between adjacent sub-sections and the environment. Conductive boundary conditions were prescribed in both the radial and z-directions for each sub-section. For the exterior surfaces, convection, radiation, and evaporative cooling conditions were assigned. For convection, the surface geometry, orientation, and speed of the wind were primary inputs for determining convective heat transfer coefficients. The cloth experiences conductive heat flows from all other contacting solid sub-sections as well as free convection from the inner chamber. This is evaluated using the temperature difference between the cloth and inner chamber. The external surface of the cloth experiences evaporation, radiation, and combined free and forced convective heat exchange. For devices containing vegetables, additional conductive heat flows between the vegetables and the inner clay pot were considered as well as free convection between the humid inner chamber air and the vegetables.

The air properties required for the Nusselt correlations were calculated at every time step using ambient temperature and humidity data using the method provided by Tsilingiris [20]. The convection Nusselt and Sherwood number correlations used are widely available in the literature [21]. The evaporation and radiation modelling approaches that form the basis of the model are detailed further in the sections below.

2.2.2. Mass balance

The net water transport from the device is determined by Eq. (2) below:

$$\frac{dN_{H_2O}}{dt} = -\sum_{i=1}^{N_s} N''_{evap,i} A_{evap,i} \tag{2}$$

where N_{H_2O} is the total amount of water stored in the device in moles, $N''_{evap,i}$ is the total evaporative molar flux from surface i, and $A_{evap,i}$ is the total surface area available for evaporation from surface i. N_s is the total number of evaporation surfaces. No volumetric water generation due to vegetable transpiration was assumed because of the high relative humidity seen within the storage chambers in Mali and Rwanda [8]. At the initial condition, the device's sand layer and cloth were assumed to be fully saturated with water. The amount of water held within the device is a function of the sand and cloth porosities and volumes. Diffusive transport within the sand layer was neglected in the model, where justification is provided in the supplementary section.

2.2.3. Evaporation model

An evaporation model was developed to quantify both the evaporation rate and its corresponding cooling effect on each evaporation surface i. These are termed $N''_{evap,i}$ and $\dot{Q}_{evap,i}$, respectively. Mathematical expressions for both $N''_{evap,i}$ and $\dot{Q}_{evap,i}$ are provided by Eq. (3) and Eq. (4), respectively. The removal of the latent heat reduces the temperature of the surface achieving the desired cooling effect [21].

$$N''_{evap,i} = \frac{h_m}{R}\left(\frac{p_{sat}(T_{s,i})}{T_{s,i}} - \frac{p_{sat}(T_\infty)}{T_\infty}RH_\infty\right) \tag{3}$$

$$\begin{aligned}\dot{Q}_{evap,i} &= \Delta H_v M_{r,H_2O} N''_{evap,i} \\ &= \frac{\Delta H_v h_m M_{r,H_2O}}{R}\left(\frac{p_{sat}(T_{s,i})}{T_{s,i}} - \frac{p_{sat}(T_\infty)}{T_\infty}RH_\infty\right)\end{aligned} \tag{4}$$

Here, h_m is the convective mass transfer coefficient and R is the universal gas constant. Within the parentheses, $p_{sat}(T_{s,i})$ is the saturation pressure of water evaluated for surface i at temperature $T_{s,i}$.

Similarly, $p_{sat}(T_\infty)$ is the saturation pressure of water evaluated at ambient conditions. The difference between these two terms accounts for the concentration difference between the evaporation surfaces and the ambient surroundings. Buck's equation was used to determine the saturation vapour pressure of water [21]. Lastly, RH_∞ is the relative humidity of the ambient environment. The surface temperature, ambient temperature, and relative humidity are all time-dependent parameters that are re-calculated or varied depending on the recorded ambient conditions at every time step. An enthalpy of vapourization for water of 2.26 MJ/kg was used and assumed to be constant for the temperature range considered [22]. The mass transfer coefficient, h_m, was calculated based on the Chilton-Colburn analogy provided by Eq. (5) [21]:

$$h_m = \frac{h}{\rho c_p \mathrm{Le}^{2/3}} \tag{5}$$

where ρ and c_p are the density and specific heat capacity of the ambient air, respectively. Le is the Lewis number. The convective heat transfer coefficient and associated fluid properties were calculated at each time step using correlations provided in the supplementary information. The evaporative transport from the surfaces of the device causes the water in the sand and cloth to deplete. The diffusive transport of water in the sand was not modelled and assumed not to bottleneck the evaporative cooling process [23]. The rate of diffusion in the sand is assumed to be faster than the rate of evaporation because based on the infinite watering case, the device is full at all instants in time. Based on field experiments, soil moisture data was also collected in addition to temperature and humidity. The data suggested that the soil was consistently wet during the course of the experiments justifying the assumption. In addition, the water in the sand was assumed not to diffuse back into the interior pots due to the high relative humidity observed within the inner chambers of both clay pot cooler variants during field trials.

2.2.4. Radiation network

Based on interviews with field staff, clay pot coolers are usually stored indoors where larger inner chamber temperature drops are achieved. Temperatures seen indoors from a radiative perspective are not the same as the ambient temperature. A radiation model was developed to emulate the environmental conditions that these coolers experience in practical settings.

Most locations where the clay pot coolers were in operation were equipped with aluminium roofs, and some having straw roofs. The radiation model inside the homes considered the radiative heat exchange between the device and the roof, ground, and walls. The surfaces were denoted as "o" for the roof and side walls, "g" for the ground, and "s" for the exterior surface of the device. The radiation resistance network can be seen in Fig. 4. An adiabatic (insulated) boundary condition was prescribed at the ground. Lastly, all surfaces were assumed to be diffuse gray emitters.

In Fig. 4, σ is the Stefan-Boltzmann constant, T_i is the temperature of surface i, A_i is the surface area of surface i, ε_i is the emissivity of surface i, and $\mathfrak{F}_{ij}$ is the view factor between surface i and surface j.

Emissivity values for each material were found based on the available literature. View factors were calculated based on a simplification that the walls of the room see the observable area fraction of the device, as seen by Eq. (6).

$$\frac{\mathfrak{F}_{so}}{\mathfrak{F}_{sg}} \approx \frac{A_o}{A_g} \tag{6}$$

Based on the radiation network in Fig. 4, all parameters are known except for the surface temperature of the device and the temperature of the roof/walls. The system of equations is iteratively solved during the solution procedure using the governing
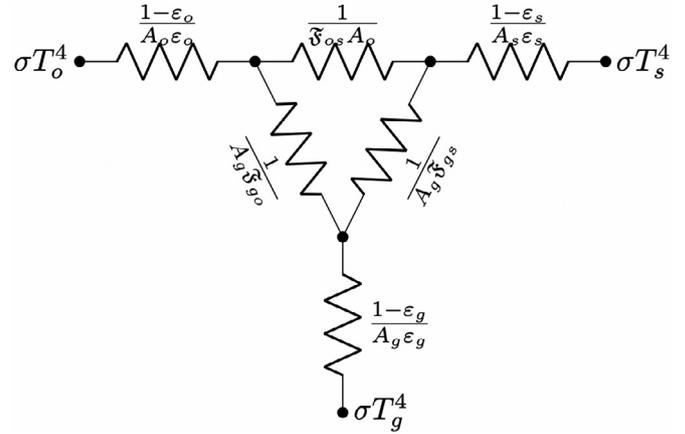

Fig. 4. Radiation network for inside the home.

equations (Eq. (1) and Eq. (2)), where the temperature of the roof/walls can be calculated as a function of the environment at each instant of time. Long-wave, short-wave incident radiation, and convection were calculated when accounting for the heat exchange with the surroundings. The effective sky temperature seen by the roof/walls from long-wave radiation is a function of the emissivity of the sky, the cloud cover, and the ambient temperature. An empirical correlation for hot and arid environments by Berdahl and Martin was used [24]. The governing relation can be found in Eq. (7) below where a is a scaled version of the dew point temperature, CC is the cloud cover, and T_∞ is the ambient temperature. During the course of the study, the value of CC was assumed to be 1.

$$T_{\mathrm{sky}} = CC(0.711 + 0.56[a + 0.73a^2]^{0.25})T_\infty \tag{7}$$

The short-wave radiation absorbed by the roof/walls was calculated as a function of the absorptivity of the roof and solar irradiation data from climates similar to those in Mali [8]. Through an energy balance a temperature of the roof/walls can be determined at a given time step.

In modelling the dwelling, a cubic room was assumed. Discussions with field staff suggested that roofs were usually made of aluminium sheets and on the order of 3.5 m tall. A roof thickness of 0.02 cm was used and emissivity values of 0.02 and 0.7 were set for the roof and the walls, respectively based on materials commonly used [8].

2.2.5. Capillary action model

For the pot-in-dish device, the modelling discussed previously transfers over with two primary modifications. The first is that a plastic dish replaces the exterior pot. The second change was motivated by an observation where a vertical capillary rise was seen on the clay pots in Mali and Rwanda. Approximately 60% of the interior clay pot's exposed surface area appeared to be wet due to water wicking up the clay from the base sand layer [6,8]. As a result, the assumption of a completely saturated pot surface needed to be modified to account for this observation.

A more restricted wetted area was determined by quantifying the height of the capillary rise process throughout the course of the simulation. A momentum balance was performed by considering all the viscous losses within the clay. The forces considered were due to capillary flow, evaporation, and Darcy's law of fluid flow in packed beds with gravitation forces. This is seen in Eq. (8) below:

$$\frac{\gamma \cos\theta_s}{R_{\mathrm{eff}}} = \rho g h_c + \frac{\varepsilon \mu h_c}{\kappa}\frac{dh_c}{dt} + \frac{\mu \pi r_2 M_{r,\mathrm{H_2O}} N''_{evap,2}}{\kappa \rho A_c} h_c^2 \tag{8}$$

→ Conductive heat flow ← → Convective heat flow ← → Radiative heat flow ← → Evaporative heat flow
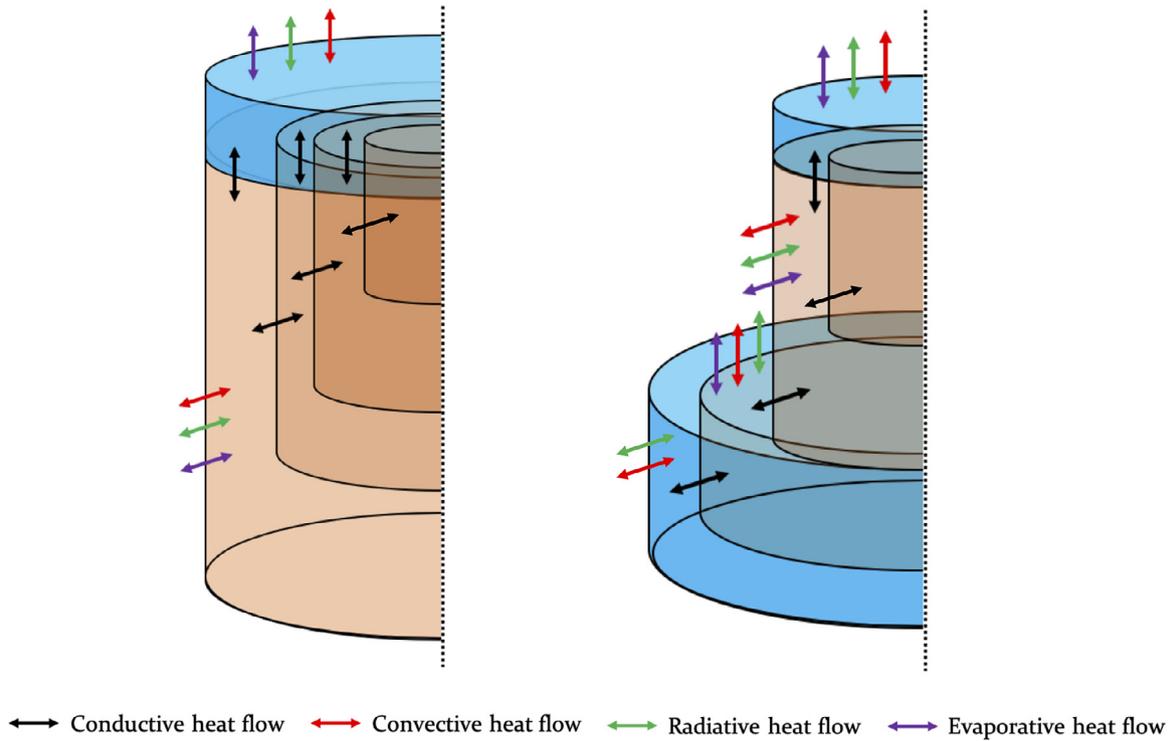
Fig. 5. Heat exchange through all modes of heat transfer for pot-in-pot and pot-in-dish systems (symmetrical about indicated axis).

where h_c is the capillary height, κ is the Darcy permeability, γ is the surface tension of water with air, θ_s is the solid contact angle, ρ is the density of water, ε is the porosity of the clay, μ is the dynamic viscosity of water, R_{eff} is the effective pore radius in the clay, and A_c is the cylindrical annulus cross sectional area of the clay pot.

The permeability of the clay was estimated using the Kozeny-Carman equation [25,26], using estimates of average porosity and pore diameter [26]. An initial condition based on the observed wetted area of 60% (~ 12 cm) was used as an input to the model. The equation was iterated along with the mass and energy conservation equations using a fourth order Runge-Kutta method to determine the transient capillary height. This solution procedure provided an effective wetted area for the clay as a function of time which was used to determine the net evaporation rate from the surface of the clay pots.

2.3. System configuration and solution procedure

In the energy balance, the conductive, convective, radiative, and evaporative heat flows are all evaluated at each time step. The primary inputs of the model are the ambient temperature and relative humidity obtained from field data. An overall system diagram showing the interfacial heat flows into and out of the system is provided by Fig. 5.

A 2–3 Runge-Kutta method was used to numerically solve the energy balance for each sub-section. The overall runtime of the model was on the order of 1 minute for a 16 day simulation (where the first 10 days of the simulation were for model equilibration and damping of transient effects, while the final 6 days were for any analysis conducted in the results and discussion section). Pot-in-dish variants required additional runtime to account for the capillary model. The solution procedure provided both temperature distributions of each sub-section and the device's water consumption as a function of time. An additional metric used to evaluate the performance of the system was the refrigeration ef-

ficiency, η_c. This term is commonly used to measure the performance of evaporative cooling devices by quantifying a normalized temperature drop. The wet bulb temperature is used to normalize the cooling effect and provides a thermodynamic minimum that can be achieved through evaporative cooling. The wet bulb temperature is calculated from experimental dry bulb temperatures and relative humidity data in conjunction with psychrometric charts [27]. The mathematical relation is found in Eq. (9) below:

$$\eta_c \equiv \frac{T_{\text{inside}} - T_\infty}{T_{\text{wet bulb}} - T_\infty} \tag{9}$$

where T_{inside} is the temperature inside the cooler, T_∞ is the ambient temperature, and $T_{\text{wet bulb}}$ is the wet bulb temperature of the ambient air. The refrigeration efficiency was calculated as a function of time to quantify cooling performance. An average efficiency was also used for average system performance, as seen by Eq. (10).

$$\tilde{\eta}_c = \frac{1}{t_{\text{end}} - t_{\text{start}}} \int_{t_{\text{start}}}^{t_{\text{end}}} \eta_c(\theta) d\theta \tag{10}$$

3. Results and discussion

3.1. Transient temperature profiles

The ambient temperature and humidity conditions from Mali and Rwanda for 17 different pot-in-pot and pot-in-dish devices were input into the model. Temperature and humidity readings were taken by DHT22 and BME280 sensors from Aosong Electronics and Bosch, respectively. Both sensors have error tolerances of $\pm$ 0.5 °C and $\pm$ 3% for temperature and relative humidity, respectively. Fig. 6 is an example of the model output for a given pot-in-pot device. The wet bulb temperature is also provided as a reference for maximum cooling. The model prediction for the inner temperature inside the chamber shows strong alignment with the experimental data. The occasional spikes noted in the experimental inner chamber temperature are due to the opening and closing of the device cover to place/remove vegetables from the inner
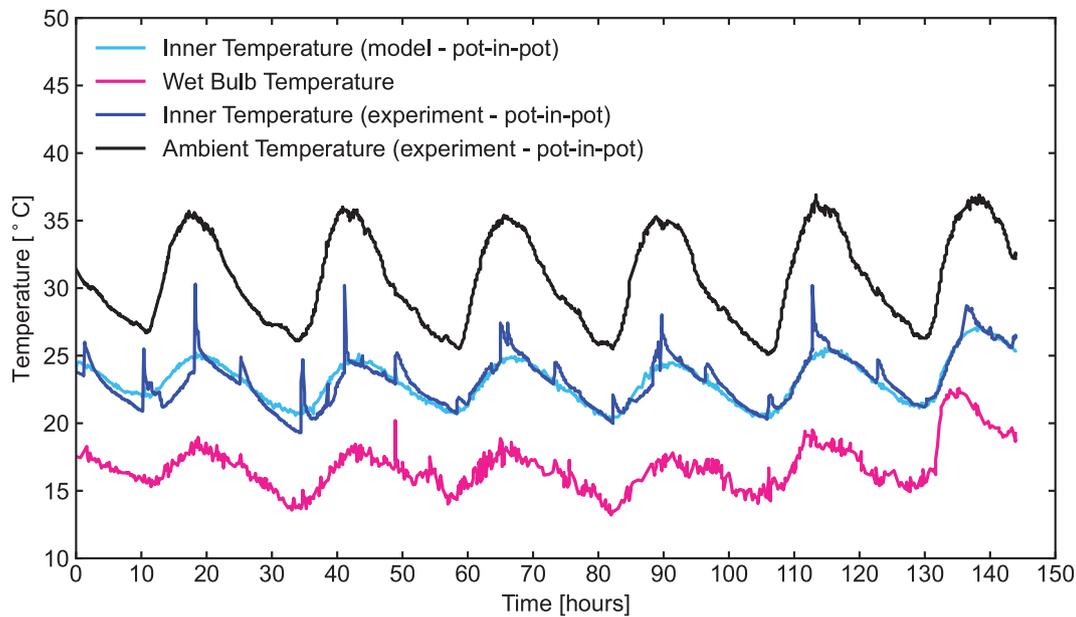
Fig. 6. Ambient, inner chamber, and wet bulb temperature variation over a 6 day period for a pot-in-pot device including model predictions (Mali).

chamber and/or add water to the device. Opening of the pot cover does not significantly impact behaviour for two reasons. Firstly, the temperature sensor is directly exposed to the ambient air and reacts quickly, however, the thermal mass of the clay pot cooler itself and the vegetables stored inside prevent significant warming of the device. Secondly, the air inside the chamber is cooler and subsequently more dense than ambient air, creating a density gradient that favours the air in remaining within the storage container. The results from the experiments support this assumption as the measured temperature returns to the original temperature prior to the cloth being removed within ~ 20 minutes. The maximum absolute percentage error (MAPE) between the model and experiments is seen to be on the order of 4% representing a maximum absolute error of 1 °C excluding data near the spikes. The MAPE was calculated by dividing the difference between the experimental results and the model outputs by the experimental results. The mean absolute error (MAE), also referred to as the time-averaged error, is an integrated average of the error over the 6 days. The value obtained is lower and averages at 0.63 °C corresponding to an average deviation of 2.5%.

Water was also sufficiently added to the device such that at no point was the device fully dry. The model assumed an infinite supply of water for all conducted model tests. The temperature of the water added to the sand and the cloth was assumed to be at thermal equilibrium with the sand and cloth, respectively at that given instant in time. Studies were conducted to determine how long it would take for the water in the device to entirely deplete (see supplementary information). The same transient temperature tests with the infinite water case were conducted on the pot-in-dish systems. The results can be observed in Fig. 7.

The model for the pot-in-dish clay pot coolers also aligns well with experiments, achieving MAPE and maximum absolute error values on the order of 6% and 1.8 °C, respectively. The MAE values for the pot-in-dish systems are higher than those observed for pot-in-pot systems and average at 0.9 °C, representing a 4% average deviation. The overall cooling achieved by the pot-in-dish coolers is lower than those observed for pot-in-pots. This is partially attributed to the decreased wetted area present in the pot-in-dish systems. In conducted tests where wetting inhabited only 60% of the inner pot, surface temperature drops varied by approximately

9.6% compared to fully wetted pot-in-dish systems. This highlights the significance of the capillary modelling. In addition, some of the cooling from the sand layer goes into cooling the dish, which does not have a mode for heat rejection through evaporation due its lower water permeability. The capillary model suggests that 60% of the clay wall serves as an evaporation surface compared to the 100% available in the pot-in-pots. The 60% value aligns well with observational data from the field where approximately 60% of the exterior pot surfaces appear wetted.

It was also noted that the wetted cloth significantly impacts the performance of pot-in-pot systems. Studies were run to characterize this behaviour by artificially setting the evaporation off the cloth to be zero and comparing the temperature drops achieved by the inner chamber in both dry and wet cloth conditions. 72% of the previously achieved temperature drop was lost using a dry cloth. This can be attributed to the number of layers observed between the ambient air and the inner storage chamber. As the cloth is the only medium separating the vegetables and the air in the z-direction, its thermal impact is more direct and noticeable. Due to the volumetric heat capacities of the sand and clay, the cooling of the exterior surfaces first cools the sand and clay before it can cool the vegetables. This is also seen in the pot-in-dish devices. The cloth only accounted for 20% of the achievable temperature drop in the pot-in-dish inner chamber in comparison to the wet cloth condition. Since the interior clay pot is freely exposed to the environment, it provides a significant amount of cooling relative to the exterior pots in the pot-in-pot configuration. Therefore, this direct contact with the inner chamber is the primary explanation for the large performance impact noted by the cloth[2]

The model output is shown for 6 days in all conducted experiments. A summary of results is provided in Table 3. Here, the range of ambient temperatures and ambient humidities from each

---

[2] Given the importance of the cloth in the cooling performance, the water depletion studies include the cloth (see supplementary section). The results suggest that the water in the cloth does not run out within the 12 h watering cycle. Instead, it is expected to take ~ 21 hours to deplete. In addition, cloth lids in the field are seen to draw moisture from the sand layer and drape over the sides of the device. Both these factors are not modelled, but add credence to the expectation that water will not run out in the cloth lid during device operation.
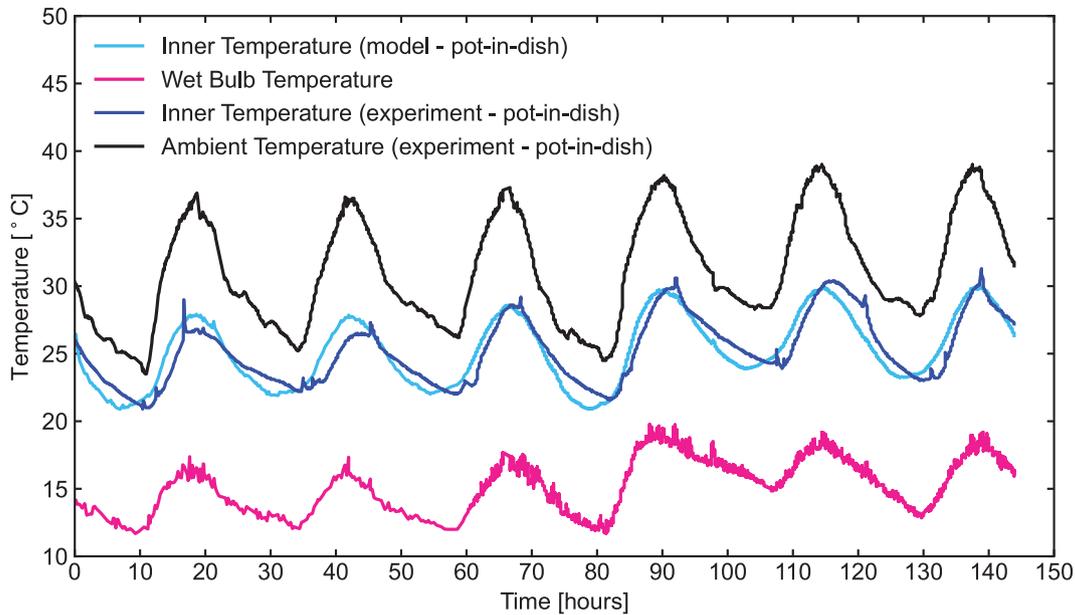
Fig. 7. Ambient, inner chamber, and wet bulb temperature variation over a 6 day period for a pot-in-dish device including model predictions (Mali).

Table 3
Summary of results with all pot-in-pot and pot-in-dish devices tested for model validation.

Location	Identifier	ΔT_{range} [°C]	RH$_{\text{range}}$ [%]	Variant	**Full** [%]	**MAE** [°C]	**Deviation** [%]	Veg. Content
Mali	s126	25.1–36.9	9.9–50.2	Pot-in-Pot	0%	0.63	2.5%	N/A
Mali	s158	25.5–38.9	9.4–65.7	Pot-in-Pot	0%	0.43	1.7%	N/A
Mali	s133	24.0–34.7	18.1–99.9	Pot-in-Pot	0%	0.67	2.6%	N/A
Mali	s112	23.5–39.8	6.4–54.0	Pot-in-Dish	0%	0.90	3.5%	N/A
Mali	s125	26.9–40.9	10.1–57.2	Pot-in-Dish	0%	0.79	3.1%	N/A
Mali	s124	24.7–38.8	14.3–75.8	Pot-in-Dish	0%	0.87	3.4%	N/A
Rwanda	Mulindi	13.3–30.0	63.6–99.9	Pot-in-Pot	29%	0.64	2.5%	Beans/chillis
Rwanda	Busago	9.5–24.2	52.8–99.9	Pot-in-Pot	28%	1.05	4.1%	Cabbage/carrots
Rwanda	Mulindi	13.7–30.7	46.0–99.9	Pot-in-Pot	30%	0.58	2.3%	Beans/chillis
Rwanda	Rubona	14.6–29.5	34.4–98.8	Pot-in-Pot	20%	0.77	3.0%	Tomatoes/chillis
Rwanda	Rubona	15.1–31.0	34.4–98.9	Pot-in-Pot	22%	0.61	2.4%	Tomatoes/chillis
Rwanda	Mulindi	13.7–30.7	46.0–99.9	Pot-in-Pot	29%	0.69	2.7%	Beans/chillis
Rwanda	Busago	9.0–25.9	36.9–99.9	Pot-in-Pot	26%	1.08	4.2%	Cabbage/carrots
Rwanda	Mulindi	13.2–31.1	61.6–99.9	Pot-in-Dish	20%	1.11	4.3%	Beans/chillis
Rwanda	Rubona	14.6–29.5	34.4–98.9	Pot-in-Pot	22%	0.74	2.9%	Tomatoes/chillis
Rwanda	Rubona	14.6–29.5	36.0–98.8	Pot-in-Dish	15%	1.30	6.5%	Tomatoes/chillis
Rwanda	Busago	9.5–25.1	52.8–99.9	Pot-in-Pot	25%	1.36	8.8%	Cabbage/carrots

location is also provided by ΔT_{range} and RH$_{\text{range}}$, respectively. In addition, the device type, average deviation, vegetable content, and device fullness is also stated. The MAPE deviation values from the devices explored in this study ranged from 1.7% to 8.8% for a wide range of ambient temperatures and ambient humidities tested, illustrating the accuracy of the model's predictive capabilities.

3.2. Refrigeration efficiency

The refrigeration efficiency as a function of time for both pot-in-pot and pot-in-dish devices in Mali is seen in Fig. 8.

As expected, the average refrigeration efficiency of the pot-in-pot systems is higher than the pot-in-dish variants. This is attributed to two primary effects. Firstly, the wet cloth covering the device is inherently smaller in pot-in-dish systems. This decreases the available area for evaporation subsequently decreasing overall system efficiency. Secondly, the water evaporating off the inner clay pot in the pot-in-dish variant comes from the wicking of water up the device from the sand layer. The capillary action results in a reduced wetted area for evaporation, while the area for radiation and convection remains unchanged. This creates a smaller

effective area for evaporation, decreasing the overall effectiveness of the device.

The difference in efficiency between both pot-in-pot and pot-in-dish devices is on the order of 15%. This value corresponds to an additional 2–3 °C drop in inner chamber temperature in pot-in-pot systems.

3.3. Water consumption

The evaporation rate from the devices for both design variants is plotted as a function of time in Fig. 9.

The trend observed for water evaporation rate suggests that the pot-in-dish systems consume more water than the pot-in-pots. This appears to be counter-intuitive given the higher refrigeration efficiency noted among the pot-in-pot devices. Further investigation showed that because the dish component of the pot-in-dish systems does not participate in evaporative heat transfer, it heats up due to convection and radiation, increasing the temperature of the adjacent sand layer. This causes more water to evaporate. The evaporation however, leads to the decrease in temperature of the dish, without a decrease in temperature of the inner storage cham-
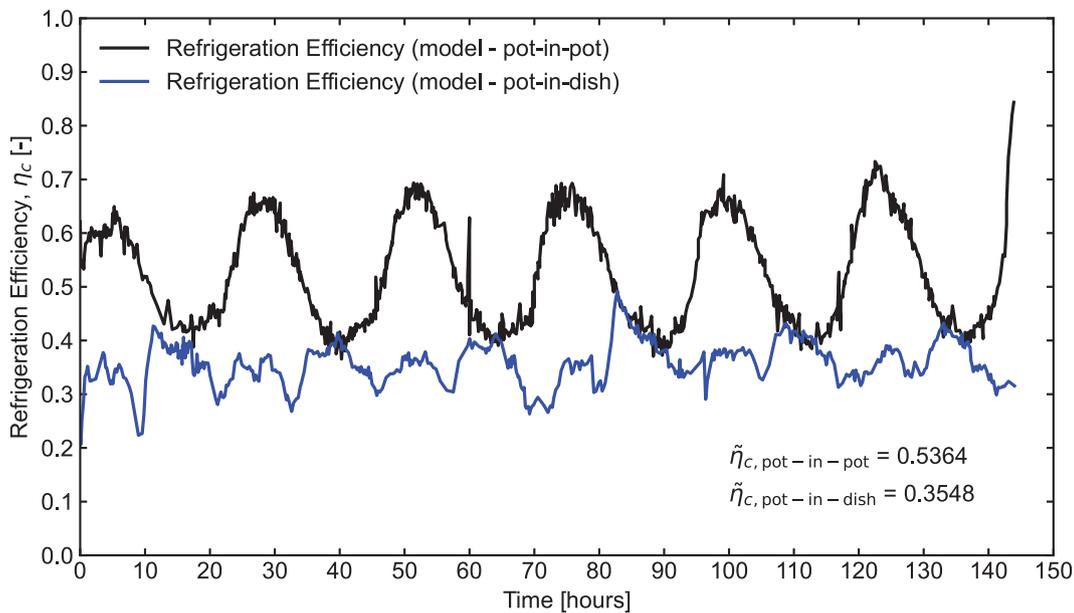
Fig. 8. The transient refrigeration efficiency of the pot-in-pot and pot-in-dish coolers (Mali).
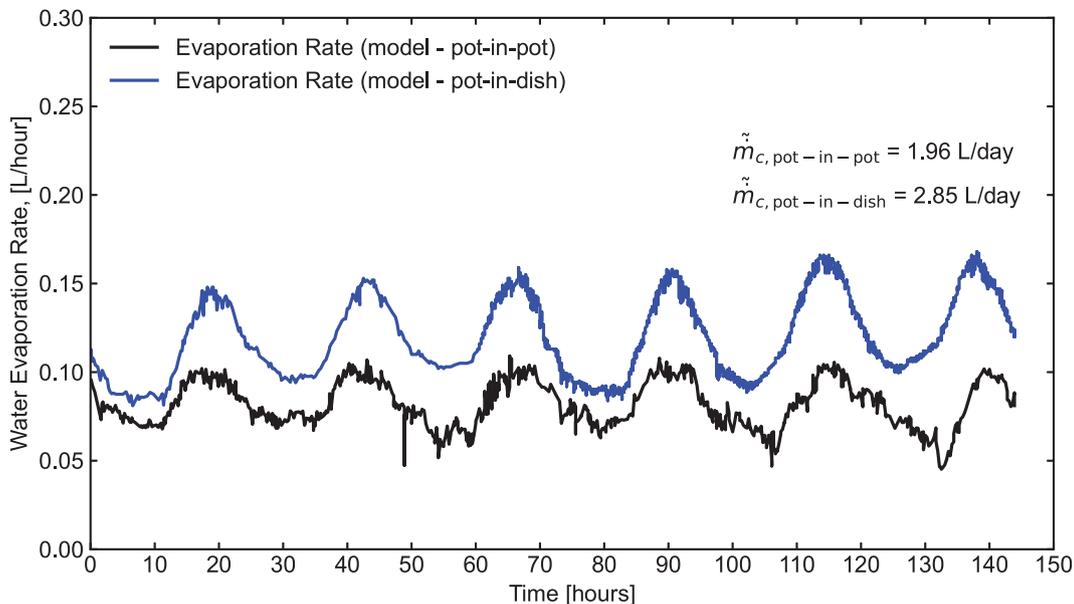

Fig. 9. The transient evaporation rate of the pot-in-pot and pot-in-dish coolers (Mali).

ber. This increases water consumption rate and yields lower refrigeration efficiencies. This process along with the lower wet bulb temperature observed in the field (due to inherent differences in ambient conditions) for the pot-in-dish systems leads to an overall 40% increase in water consumption of the pot-in-dish systems as noted in Fig. 9. Therefore, despite the decrease in effective area for evaporation within the pot-in-dish devices, this is offset by the adverse impact of the plastic dish explaining the observed trend.

3.4. Parametric studies

3.4.1. Variations in wind speed

In experiments, it was observed that the coolers were sensitive to wind speed. Wind speed was varied in the model to see the impact on time-averaged refrigeration efficiency and daily water consumption. The ambient temperature and relative humidity used

in these studies is consistent with those observed in Sections 3.1, 3.2, and 3.3. The results are provided in Fig. 10 and Fig. 11. The study considered wind speeds ranging from 0.2–10 m/s, reflecting air speeds seen in both typical indoor conditions and fresh outdoor breezes [28,29].

As the wind speed is increased, both clay pot coolers cool more effectively. The increase in efficiency observed in Fig. 10 is primarily localized to speeds ranging from 0 to 3 m/s where beyond that diminishing returns are observed. The shapes of the curves are also expected as the variation of the convective heat and mass transfer coefficients varied as a function of Reynolds number to the one half power. More importantly, although increasing wind speed leads to more convective heating, the increase in cooling achieved is still large enough to offset the negative impact of increased convective heat transfer. The increased cooling is also a result of additional water evaporating from the surfaces of the devices validated by the similar trend noted in Fig. 11.
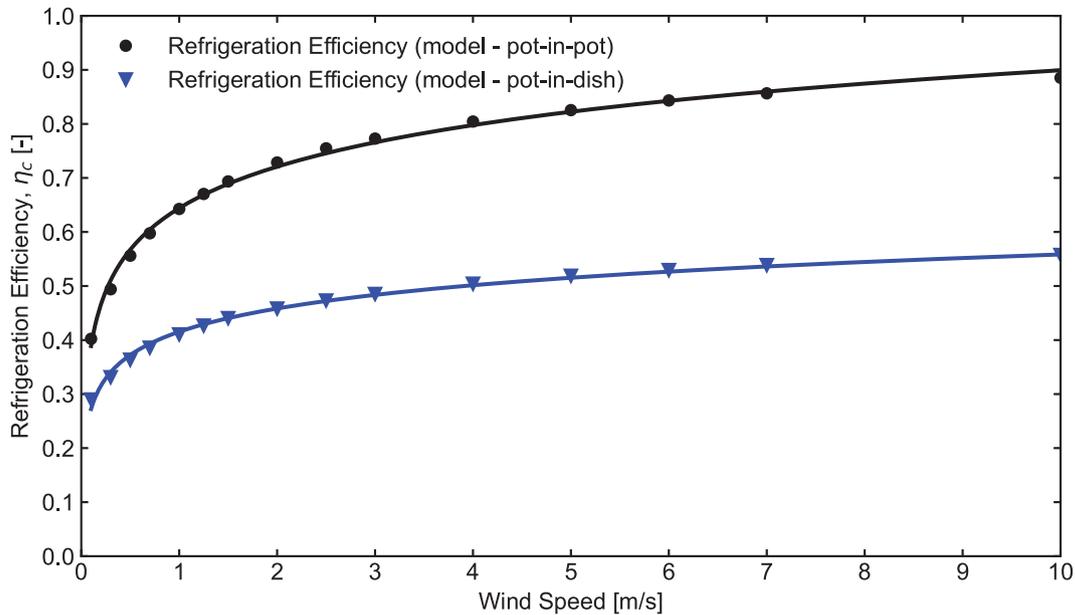
Fig. 10. Variation in refrigeration efficiency as a function of wind speed. Logarithmic fits included to fit curve to the modelling results for pot-in-pot and pot-in-dish systems.
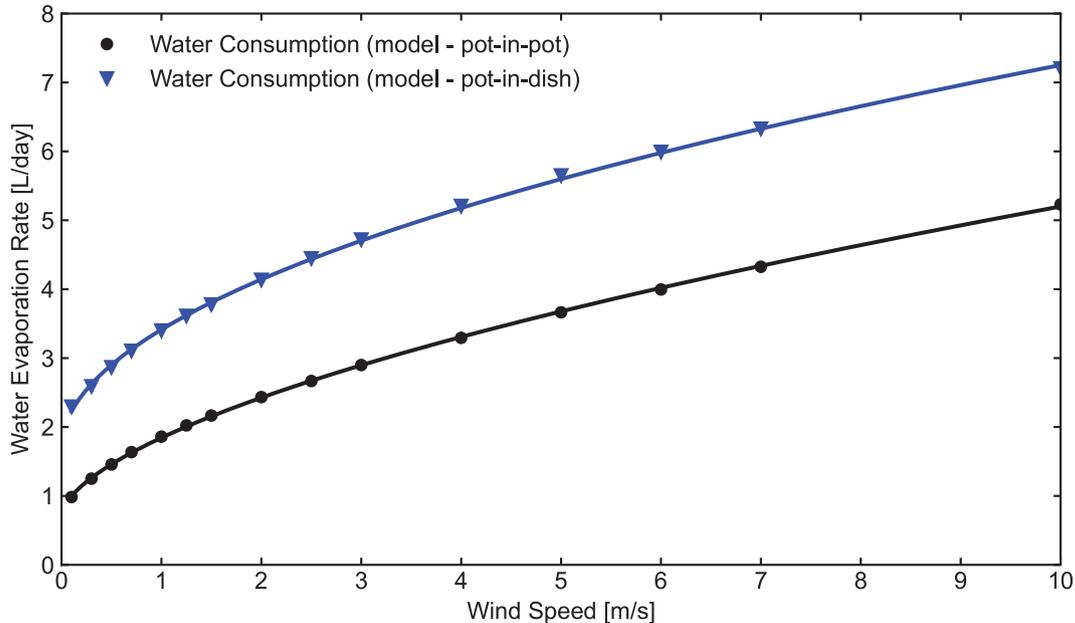
Fig. 11. Variation in daily water consumption as a function of wind speed. Power fits included to fit curve to the modelling results for pot-in-pot and pot-in-dish systems.

3.4.2. Variations in size and chamber contents

Studies were conducted to investigate the impact of vegetable storage inside the inner chamber on system performance. Vegetables used included tomatoes, French beans, chilli peppers, cabbage, or carrots, depending on the specific device deployed. The chamber's volumetric contents (as a percentage) and the overall size of the device were varied as independent parameters to predict the impact on average refrigeration efficiency and daily water consumption. The size of the device was scaled by increasing each material's thickness, the inner pot radii, and the device's height by the same scaling factor. Results from these studies are illustrated in Fig. 12 and Fig. 13 for pot-in-pot systems.

As a pot-in-pot device of a given size is increasingly filled with vegetables, the refrigeration efficiency decreases. Increasing the contents of the inner chamber leads to more energy being required to cool the vegetables stored inside. Since the evaporative

driving force remains virtually unchanged, the impact is noticed on the refrigeration efficiency.

As the pot-in-pot increases in size for a given a vegetable content, the efficiency of the device is seen to initially drop until it reaches a minimum. For pot-in-pot systems that are smaller in scale, the evaporative cooling driving force is more than sufficient to supply the necessary cooling for the chamber contents. The impact of small available area for evaporation is not able to offset the cooling phenomenon. As the pot-in-pot increases in size, the driving force stays relatively constant, but the contents require more energy to cool. This leads to the decreasing refrigeration efficiency observed in Fig. 12. As the thermal mass grows for increasing pot-in-pot sizes, so does the available surface area for evaporation. These competing effects reach a balance at the minimum point observed in Fig. 12. As the size of the pot-in-pot is increased beyond this point, the increase in evaporation due to the available surface
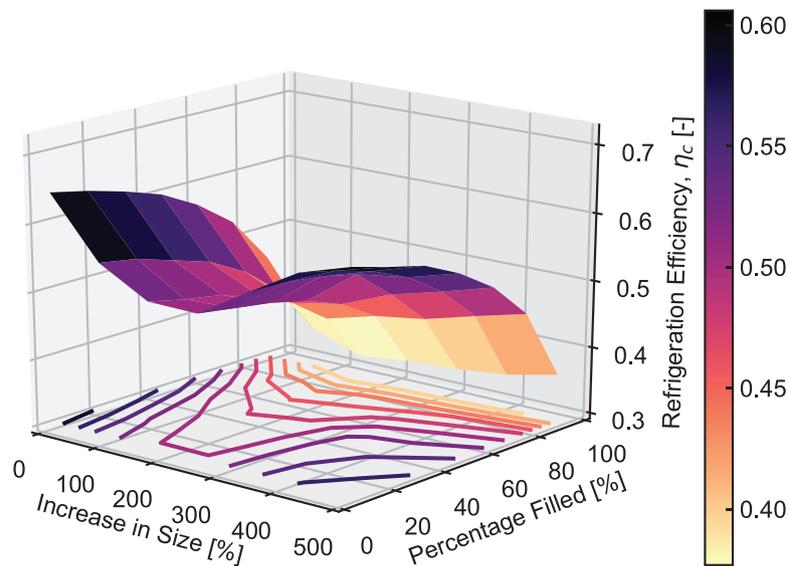
Fig. 12. Variation in refrigeration efficiency as a function of vegetable content and percentage increase in device size for a pot-in-pot system.
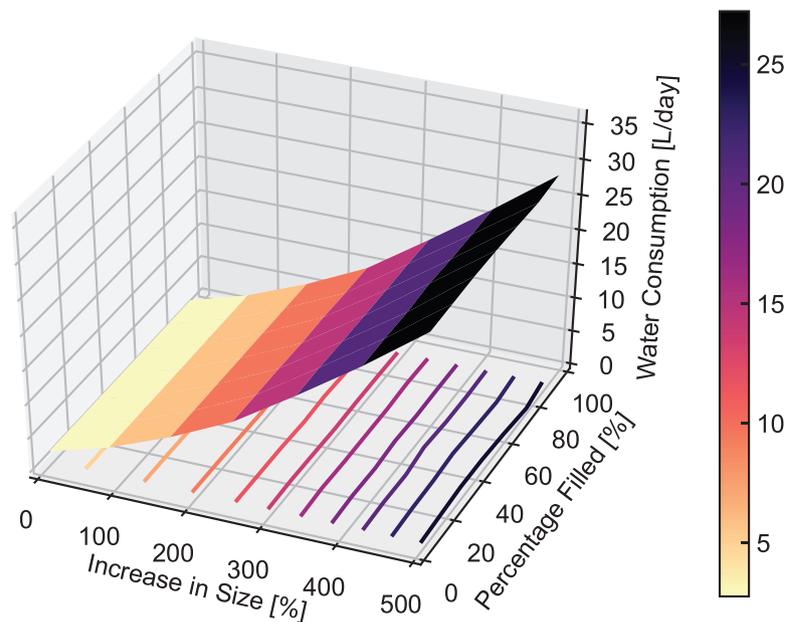

Fig. 13. Variation in water consumption as a function of vegetable content and percentage increase in device size for a pot-in-pot system.

area for evaporation is large enough to offset the decrease in efficiency due to the thermal mass. This justifies the increase in refrigeration efficiency noted past the minimum point, highlighting the gains in device efficiency upon system scale-up.

For water consumption rates, the trends are primarily explained by the increased available area for evaporation. As the pot-in-pot size increases, the evaporative driving force remains relatively constant, but the available surface area for evaporation increases. The product of these two effects leads to increasing water consumption as there is more available area for water to evaporate off. For a fixed pot-in-pot size, since this driving force and evaporative surface area remains relatively unchanged, the impact of adding vegetables to the system is seen by the reduced refrigeration efficiency discussed earlier and not a variation in water consumption. This suggests that the efficacy of the cooling is captured by the refrigeration efficiency, but the net amount of water evaporated is a byproduct of the available surface area for evaporation. In addition, these results allude to the relatively decoupled nature

and independence of these parameters. As the vegetable filling percentage inside the inner chamber is increased, the increased conductive heat flows remain much smaller in magnitude in comparison to the evaporative, radiative, and convective heat flows on the outer pot and cloth. Consequently, the evaporation rate remains virtually unchanged by the amount of mass in the inner chamber.

A similar analysis was carried out for pot-in-dish systems and is presented by Fig. 14 and Fig. 15 below. The same trend in refrigeration efficiencies noted previously is observed in the pot-in-dish variants with a minimum refrigeration efficiency achieved for a specific device size. The reasoning provided for the pot-in-pot systems carries over. The interplay between the thermal mass and surface area for evaporation creates an inherent trade-off. This yields the minimum value observed. The pot-in-dish variants are slightly more sensitive to filling than pot-in-pots. For a given size, the efficiency is seen to either increase or decrease depending on the system size.
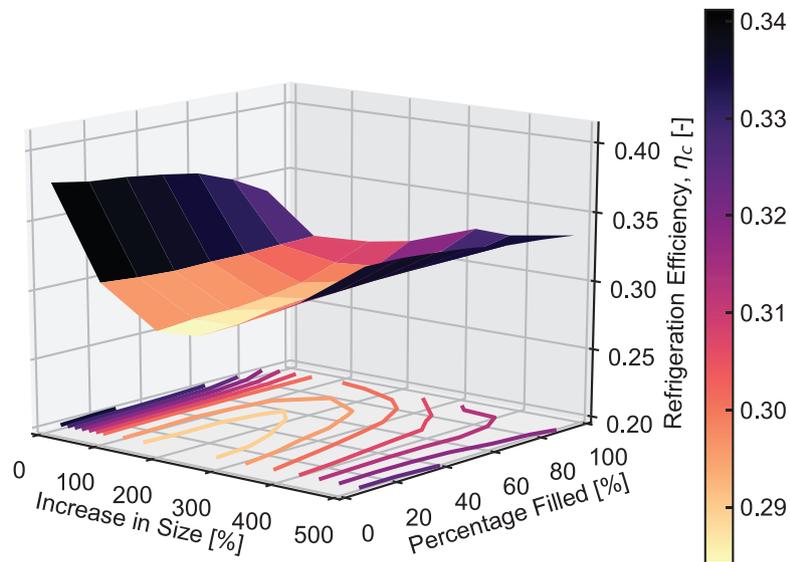
Fig. 14. Variation in refrigeration efficiency as a function of vegetable content and percentage increase in device size for a pot-in-dish system.
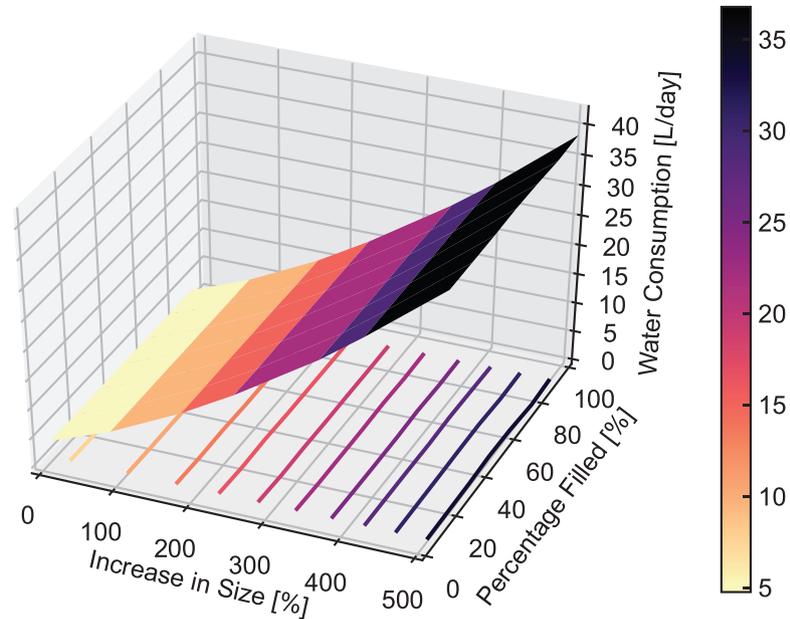

Fig. 15. Variation in water consumption as a function of vegetable content and percentage increase in device size for a pot-in-dish system.

Similarly with water consumption, the pot-in-dish systems exhibit the same behaviour as the pot-in-pots. This result justifies the decoupled nature of the refrigeration efficiency and water consumption. It suggests that increasing surface area, which increases water consumption, does not necessarily yield better performance for a given device variant. Therefore, the highest refrigeration efficiency attainable for the smallest surface area would provide the largest savings in water. Storage volume must also be sufficient for a significant quantity of vegetables to be stored. This intrinsic trade-off requires further studies to be conducted to investigate the optimal design of these systems.

4. Conclusion

This study details a mechanistic heat and mass transport model that predicts the performance of pot-in-pot and pot-in-dish devices deployed in the African Sahel region. Using data obtained from service environments in Mali and Rwanda for multiple device variants, this study validates the formulated model. Key contributions include:

- Transient temperature profiles from the model are in agreement with the observed temperatures from the field. Maximum deviations over the 6 day simulation were 8.8% and 6.5% for pot-in-pot and pot-in-dish systems, respectively.
- A parametric study evaluated the impact of wind speed, overall device size, and inner chamber content on water consumption and refrigeration efficiency.
- 32% and 30% of device cooling originates from the cloth lid for pot-in-pot and pot-in-dish configurations, respectively.
- The impact of wind speed on device performance experiences diminishing returns beyond wind speeds of 3 m/s.
- Maintaining a wet cloth is critical in maximizing the device's temperature drop. A dry cloth reduces the temperature drop achieved by the inner chamber by 72% for pot-in-pot devices.

- Increasing device size illuminates a tradeoff between the impacts of thermal mass and larger evaporative surface area on refrigeration efficiency: Smaller devices are negatively impacted by size increases via a thermal mass effect, while larger devices achieve improved refrigeration efficiencies due to an increased evaporative surface area.
- Increasing the vegetable load in the device showed virtually no change in the water consumption of the devices.

Declaration of Competing Interest

The authors declare that they have no known competing financial interests or personal relationships that could have appeared to influence the work reported in this paper.

CRediT authorship contribution statement

Acknowledgements

Supplementary material

Supplementary material associated with this article can be found, in the online version, at doi:10.1016/j.ijheatmasstransfer.2020.120270.

References

[1] X. Zhao, S. Liu, S.B. Riffat, Comparative study of heat and mass exchanging materials for indirect evaporative cooling systems, Build. Environ. 43 (11) (2008) 1902–1911, doi:10.1016/j.buildenv.2007.11.009. ISSN 0360-1323.

[2] V.M. Nguyen, S.B. Riffat, P.S. Doherty, Development of a solar-powered passive ejector cooling system, Appl. Therm. Eng. 21 (2) (2001) 157–168, doi:10.1016/S1359-4311(00)00032-6. ISSN 1359-4311.

[3] A. lal Basediya, D.V.K. Samuel, V. Beera, Evaporative cooling system for storage of fruits and vegetables - A review, J. Food Sci. Technol. 50 (3) (2013) 429–442, doi:10.1007/s13197-011-0311-6. ISSN 0022-1155.

[4] J. Kuo, D. Rehman, D.A. Romero, C.H. Amon, A novel wake model for wind farm design on complex terrains, J. Wind Eng. Ind. Aerodyn. 174 (2018) 94–102, doi:10.1016/j.jweia.2017.12.016. ISSN 0167-6105.

[5] W. Breslyn, Clay pot refrigerators, Sci. Teach. 74 (8) (2007) 74. https://www.questia.com/library/journal/1G1-172598350/clay-pot-refrigerators.

[6] E. Verploegen, O. Sanogo, T. Chagomoka, Evaluation of low-cost evaporative cooling technologies for improved vegetable storage in Mali, in: 2018 IEEE Global Humanitarian Technology Conference (GHTC), 2018, pp. 1–8, doi:10.1109/GHTC.2018.8601894.

[7] Y.D. Ahdab, D. Rehman, J.H. Lienhard, Brackish water desalination for greenhouses: Improving groundwater quality for irrigation using monovalent selective electrodialysis reversal, J. Membrane Sci. 610 (2020) 118072, doi:10.1016/j.memsci.2020.118072. ISSN 0376-7388.

[8] E. Verploegen, O. Sanogo, T. Chagomoka, Evaporative cooling technologies for improved vegetable storage in Mali, MIT D-Lab, 2018. http://hdl.handle.net/1721.1/116211.

[9] O. Oluwasola, Pot-in-pot enterprise: Fridge for the poor, United Nations Development Programme (2011) 1–18. http://growinginclusivemarkets.org/media/cases/Nigeria_PotInPot_2011.pdf.

[10] L. Jaconelli, K.J. Palm, A thermal network model for an evaporative cooling system combined with a solar chimney, 2016. https://www.diva-portal.org/smash/record.jsf?pid=diva2%3A971809.

[11] B.N. Nwankwojike, O.S. Onwuka, P.T. Anukam, F.I. Abam, H.N. Chilaka, Mechanistic modeling of water replenishment rate of zeer refrigerator, Arid Zone J. Eng. Technol. Environ. 13 (3) (2017) 369–379. https://www.researchgate.net/publication/318828058_Mechanistic_Modeling_of_Water_Replenishment_Rate_of_Zeer_Refrigerator.

[12] A. Date, Heat and mass transfer analysis of a clay-pot refrigerator, Int. J. Heat Mass Transf. 55 (15) (2012) 3977–3983, doi:10.1016/j.ijheatmasstransfer.2012.03.028.

[13] L. Yanhua, L. Enli, M.M. Rahman, W. Yu, G. Jiaming, Z. Jie, Numerical simulation of temperature and relative humidity in zero energy cool chamber, Int. J. Agric. Biol. Eng. 10 (3) (2017) 185–193, doi:10.3965/j.ijabe.20171003.3050.

[14] E. Verploegen, R. Ekka, G. Gurbinder, Evaporative cooling for improved vegetable and fruit storage in Rwanda and Burkina Faso, 2019. https://hdl.handle.net/1721.1/121582.

[15] I.N. Hamdhan, B.G. Clarke, Determination of thermal conductivity of coarse and fine sand soils, in: Proceedings of World Geothermal Congress, 2010, pp. 1–7. https://pdfs.semanticscholar.org/6000/3077b4d26d340b541ca63589b393479d30bd.pdf.

[16] M. Slavinec, R. Repnik, E. Klemenčič, The impact of moisture on thermal conductivity of fabrics, Anali Pazu 6 (1-2) (2016) 8–12. http://www.anali-pazu.si/sites/default/files/Slavinec%20M.%20et%20al_2.pdf.

[17] M. Sutcu, J. Diaz, F. Rabanal, O. Gencel, S. Akkurt, Thermal performance optimization of hollow clay bricks made up of paper waste, Energy Build. 75 (2014) 96–108, doi:10.1016/j.enbuild.2014.02.006. ISSN 0378-7788.

[18] C. Liu, J. Wang, J. He, Rheological and thermal properties of m-LLDPE blends with m-HDPE and LDPE, Polymer 43 (13) (2002) 3811–3818, doi:10.1016/S0032-3861(02)00201-X. ISSN 0032-3861.

[19] B. Sajjadi, A.A.A. Raman, H. Arandiyan, A comprehensive review on properties of edible and non-edible vegetable oil-based biodiesel: Composition, specifications and prediction models, Renew. Sust. Energ. Rev. 63 (2016) 62–92, doi:10.1016/j.rser.2016.05.035. ISSN 1364-0321.

[20] P.T. Tsilingiris, Thermophysical and transport properties of humid air at temperature range between 0 and 100°C, Energ. Convers. Manage. 49 (5) (2008) 1098–1110, doi:10.1016/j.enconman.2007.09.015. ISSN 0196-8904.

[21] F.P. Incropera, D.P. DeWitt, Fundamentals of Heat and Mass Transfer, John Wiley & Sons, Inc., Hoboken, NJ, USA, 2006. ISBN 0470088400. https://dl.acm.org/doi/book/10.5555/1209497.

[22] V. Majer, V. Svoboda, J. Pick, Heats of Vaporization of Fluids, Developments in Crop Science, Elsevier, 1989. ISBN 9780444417626. https://books.google.com/books?id=aot6AAAAIAAJ.

[23] M.M. Elhalwagy, A.G. Straatman, Dynamic coupling of phase-heat and mass transfer in porous media and conjugate fluid/porous domains, Int. J. Heat Mass Tran. 106 (2017) 1270–1286, doi:10.1016/j.ijheatmasstransfer.2016.10.108. ISSN 0017-9310.

[24] J.H. Lienhard IV, J.H. Lienhard V, A Heat Transfer Textbook, 5th, Phlogiston Press, Cambridge, MA, 2019. Version 5.00.

[25] P. Xu, B. Yu, Developing a new form of permeability and Kozeny-Carman constant for homogeneous porous media by means of fractal geometry, Adv. Water Resour. 31 (1) (2008) 74–81, doi:10.1016/j.advwatres.2007.06.003. ISSN 0309-1708.

[26] W.M. Deen, Introduction to Chemical Engineering Fluid Mechanics, Cambridge Series in Chemical Engineering, Cambridge University Press, 2016, doi:10.1017/CBO9781316403464.

[27] 2011 ASHRAE Handbook Heating, Ventilating, and Air-conditioning Applications, ASHRAE, Atlanta, GA, SI edition. ISBN 9781613446652. https://www.academia.edu/22524538/2011_ASHRAE_HANDBOOK_HVAC_Applications_SI_Edition.

[28] M. Monmonier, Defining the wind: the beaufort scale, and how a 19th century admiral turned science into poetry, Prof. Geogr. 57 (3) (2005) 474–475, doi:10.1111/j.0033-0124.2005.493_1.x.

[29] A.S. Hassan, M. Ramli, Natural ventilation of indoor air temperature: a case study of the traditional Malay house in Penang, Am. J. Eng. Appl. Sci. 3 (3) (2010) 521–528, doi:10.3844/ajeassp.2010.521.528.